Particle Image Velocimetry Measurements of a Two/Three-dimensional Separating/Reattaching Boundary Layer Downstream of an Axisymmetric Backward-facing Step

Laura M. Hudy* and Ahmed M. Naguib†
Michigan State University, East Lansing, MI-48824

William M. Humphreys‡ and Scott M. Bartram§
NASA Langley Research Center, Hampton, VA-23681

Planar Particle Image Velocimetry measurements were obtained in the separating/reattaching flow region downstream of an axisymmetric backward-facing step. Data were acquired for a two-dimensional (2D) separating boundary layer at five different Reynolds numbers based on step height (Re_h), spanning 5900-33000, and for a three-dimensional (3D) separating boundary layer at Re_h = 5980 and 8081. Reynolds number effects were investigated in the 2D cases using mean-velocity field, streamwise and wall-normal turbulent velocity, and Reynolds stress statistics. Results show that both the reattachment length (x_r) and the secondary separation point are Reynolds number dependent. The reattachment length increased with rising Re_h while the secondary recirculation region decreased in size. These and other Re_h effects were interpreted in terms of changes in the separating boundary layer thickness and wall-shear stress. On the other hand, in the 3D case, it was found that the imposed cross-flow component was relatively weak in comparison to the streamwise component. As a result, the primary influences of three dimensionality only affected the near-separation region rather than the entire separation bubble.

Nomenclature

h	=	step height
Re	=	Reynolds number
Re_h	=	Reynolds number based on step height
Re_θ	=	Reynolds number based on momentum thickness of the separating boundary layer
u_{rms}	=	root-mean-squared of streamwise velocity component
$\overline{u'v'}$	=	Reynolds shear stress
u_τ	=	friction velocity
U_∞	=	freestream velocity
v_{rms}	=	root-mean-squared of normal velocity component
w_{rms}	=	root-mean-squared of streamwise velocity component
W_s	=	transverse velocity of the rotator surface
x	=	streamwise coordinate
x_r	=	reattachment length
y	=	wall-normal coordinate
y^+	=	wall-normal coordinate normalized by friction velocity and kinematic viscosity
z	=	spanwise coordinate
δ_{99}	=	99% boundary layer thickness

* Graduate Student, Department of Mechanical Engineering, C130 RCE, and AIAA Member.
† Associate Professor, Department of Mechanical Engineering, C128 RCE, and AIAA Member.
‡ Research Engineer, Aeroacoustics Branch, M/S 461, and Senior AIAA Member.
§ Engineering Technician, Advanced Sensors and Optical Measurements Branch, M/S 493.

θ = momentum thickness of the boundary layer at separation

I. Introduction

One important class of fluid flow that is encountered frequently in aerospace applications is that of separated flows. These applications include flow over airplane wings and through turbines and compressors, to mention a few. Extensive research has been done in the area of separated flows in order to understand the dominant flow structures in the separated shear layer and the general characteristics of the flow field. The ability to understand the flow field can lead to the development of active or passive flow control techniques for optimizing the flow state above the surface. Flow control has been an active research area over the past decade and studies have shown the ability of control techniques to improve the performance of, for example, wings by maximizing lift and minimizing drag[1]. Nonetheless, further research in the area of separated flows as well as the mechanisms for controlling the flow is needed. This is particularly true when the controlled flow involves non-canonical, complicating factors such as three-dimensionality, curvature, wall-roughness, etc.

An example of a canonical separated-flow configuration is the backward-facing step (BFS) geometry shown in Fig. 1. This flow is frequently adopted for the purpose of research studies as an idealization of real separated flow problems. Generally speaking, flow separation occurs where the flow detaches from the boundary of a solid surface, which is at the step edge in the case of the BFS. When the boundary layer separates it forms a shear layer that may reattach along the same surface depending on the length and contour of the geometry. Beneath the shear layer is a primary and a secondary re-circulating region. Once the boundary layer separates, the flow becomes highly unstable. As a result, large-scale turbulent structures develop in the shear layer, growing in size and strength as they convect downstream towards reattachment. Beyond the reattachment point, the reattached boundary layer begins to relax as it redevelops into an equilibrium turbulent boundary layer for a sufficiently long surface.

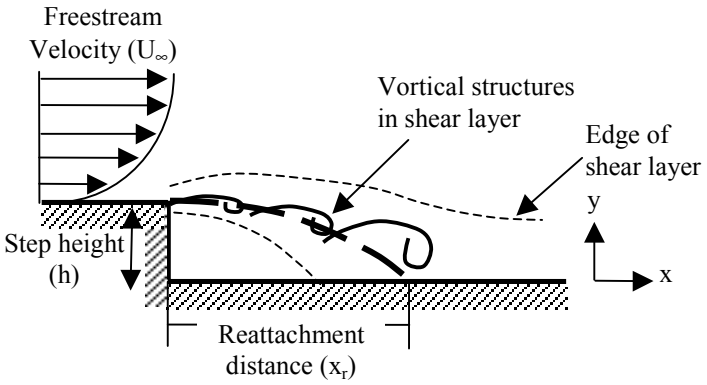

Figure 1. Example of separated flow in a backward-facing step

The current research project investigated the separation/reattachment of both a two-dimensional (2D) and three-dimensional (3D) boundary layer over an axisymmetric backward-facing step (BFS). Most of the separating/reattaching flow research to date has been on 2D flows in planar classical geometries such as a backward-facing step, a splitter plate, or a splitter-plate-with-fence. These studies include, but are not exclusive to, Eaton and Johnston[2] (BFS), Cherry *et al.* [3] (splitter plate), Castro and Haque[4] (splitter-plate-with-fence), and many others. In these studies, mean flow two-dimensionality was assumed due to the large aspect ratio (width of the model divided by the step height). Since the geometries were not infinitely wide and ended abruptly at the sidewalls, the effects of the sidewalls resulted in the mean flow inherently not being 2D. In the case of the axisymmetric configuration, there are no sidewalls and therefore, the mean flow is truly 2D due to invariance in the azimuthal direction. Some authors have also investigated 3D separated flows, which is more characteristic of real world situations, although the scope of this research is limited. One such study was completed by Hancock and McClusky[5] in 1997. They used a swept fence in a splitter plate configuration to create a spanwise-invariant 3D separated flow in which they measured mean velocity and Reynolds stresses. Nonetheless, because of the splitter plate configuration it is difficult to compare 2D and 3D cases. Driver and Hebbar[6] is another example study. In 1989, the two authors explored the effects of adverse pressure gradient on a 3D boundary layer using a forward-facing step in an axisymmetric geometry. They recorded mean flow, Reynolds stresses, and velocity triple-product correlations in the flow field. However, in the Driver and Hebbar[6] study the separation point location was unsteady; whereas, with the current project 3D

separation is occurring over a 2D geometry (invariance in azimuthal direction) with known separation point at the step. This simplifies the problem, eliminating some of the unknowns and allowing for the focus to be on the flow field beyond separation.

Li and Naguib[7] investigated Reynolds number effects in the same axisymmetric backward-facing step model employed here (see the Experimental Set-up, Section II for more details) using a high-frequency oscillating hot-wire sensor that measured the wall-shear stress. The sensor was embedded in the wall of the model at different streamwise positions spanning 0.3 to 10 step heights downstream of the step edge and measured both skin friction magnitude and direction. Data were acquired within the viscous sublayer at a height of 97 μm above the wall, which corresponds to a $y^+ = 3.1$. The skin friction measurements were used to characterize the flow surrounding the axisymmetric BFS and to compare results with existing planar BFS studies. One fundamental quantitative difference Li and Naguib[7] found was that the data in the axisymmetric geometry revealed a shorter reattachment length compared to planar BFS studies. Li and Naguib[7] attributed this to the difference in geometry. In addition, Li and Naguib[7] also observed that over the Reynolds number range investigated (Re_h = 4300-13000; based on step height) the reattachment length increased slightly with increasing Reynolds number. This growth in x_r was explained to be the result of a decrease in the boundary layer thickness, which has been sited in literature by both Eaton and Johnston[2] and Adams and Johnston[8].

Spazzini *et al.*[9] observed the same trend in their investigation of the unsteady behavior in a planar BFS at Reynolds numbers based on step height spanning 3500-16000. The group obtained time-resolved skin-friction measurements using a wall-mounted double hot-wire probe. Digital PIV measurements were also acquired in a companion experiment completed in a water tunnel. These measurements provided quantitative information about the flow field as well as qualitative visualizations. Data from both measurement techniques revealed a strong dependence between x_r and Re_h with the length of reattachment growing with increasing Reynolds number. In addition, Spazzini *et al.*[9] found that the location of the secondary separation point was weakly dependent on Reynolds number. The group observed that the location of the secondary separation point moved closer to the step with rising Reynolds number.

Kostas *et al.*[10] acquired PIV measurements in a planar backward-facing step geometry at Re_h = 4660. From their measurements, the mean velocity field in the plane-of-view parallel to the streamwise and wall-normal coordinates revealed both primary and secondary recirculation regions. The mean reattachment point recorded was 4.8h ± 0.2h, which Kostas *et al.*[10] stated could not be accurately obtained because the PIV data did not extend to the wall. In addition, Kostas *et al.*[10] found x_r to be shorter than reported in literature and they attributed this to the high level of turbulence levels near the wall in the upstream boundary layer. Reynolds stress components $\overline{u'^2}, \overline{v'^2}, \overline{u'v'}$ normalized by U_∞^2 were also presented. Kostas *et al.*[10] found appreciable Reynolds stress values starting around two step heights downstream of separation at a vertical height of y = h. The group also reported that the largest levels of Reynolds stress were located upstream of reattachment. The maximum values occurred roughly one step height upstream of reattachment at a y = 0.7h height. Beyond reattachment, Kostas *et al.*[10] observed a decline in the Reynolds stress levels.

Scarano and Riethmuller[11] published a study describing an improved algorithm for interrogating PIV images. In the paper, they presented PIV data in the form of mean velocity and Reynolds stress quantities from a planar backward-facing step study at Re_h = 5000. The mean velocity profiles with streamlines show both a primary and secondary re-circulation region and a reattachment distance of x_r = 5.9h. Reynolds stress contour maps show that the maximum values observed for u_{rms}, v_{rms} and $\overline{u'v'}$ were located along the centerline of the shear layer. Scarano and Riethmuller[11] found the maximum u_{rms} value of 17% of the freestream velocity to be approximately one step height upstream of x_r. As for v_{rms} and $\overline{u'v'}$, the maximum values occurred at x/h = 5 and had a magnitude of 12% and 1.2%, respectively, when normalized using U_∞.

Although the backward-facing-step flow field has been investigated extensively over the past few decades, the majority of these studies have utilized time, rather than space, resolved measurements. Only during the last decade have a few PIV studies of the BFS flow become available. All of these have been conducted in a planar flow geometry, which suffers from the inability to establish a truly two-dimensional mean flow because of end effects as mentioned above. The objective of this study is to explore the statistics of the velocity flow field above the surface using PIV measurements in a geometry that allows for truly 2D as well as 3D separating boundary layer conditions. This information will give better understanding of the flow structures that develop in the shear layer beyond separation as well as provide a database that is suitable for benchmarking of computational codes based on periodic boundary conditions. Additionally, wall-pressure-array data and two-point wall-shear-stress information have been acquired in the same flow geometry. The collective data set provides a unique combination of information not available before in the investigated flow. It should be noted, however, that this paper presents only a portion of the

PIV data and investigates the Reynolds number effect on the flow for the two-dimensional separating boundary layer case. In addition, a comparison is made between the two-/three-dimensional cases at a Reynolds number of 8081 (U_∞ = 10 m/s).

II. Experimental Set-up

The experiment was completed in the Subsonic Basic Research (Wind) Tunnel at NASA Langley Research Center in Hampton, Virginia. The open-circuit, low-speed wind tunnel has a 6:1 contraction ratio upstream of a 0.57 m-wide by 0.84 m-high by 1.85 m-long test section. An adjustable false floor was placed in the test section and was set at a slight angle so that the pressure gradient in the test section was zero. The nominal height of the test section with the false floor installed was 0.62 m. The axisymmetric backward-facing step model shown in Fig. 2 was centered between the sidewalls, the ceiling, and the false floor within the test section.

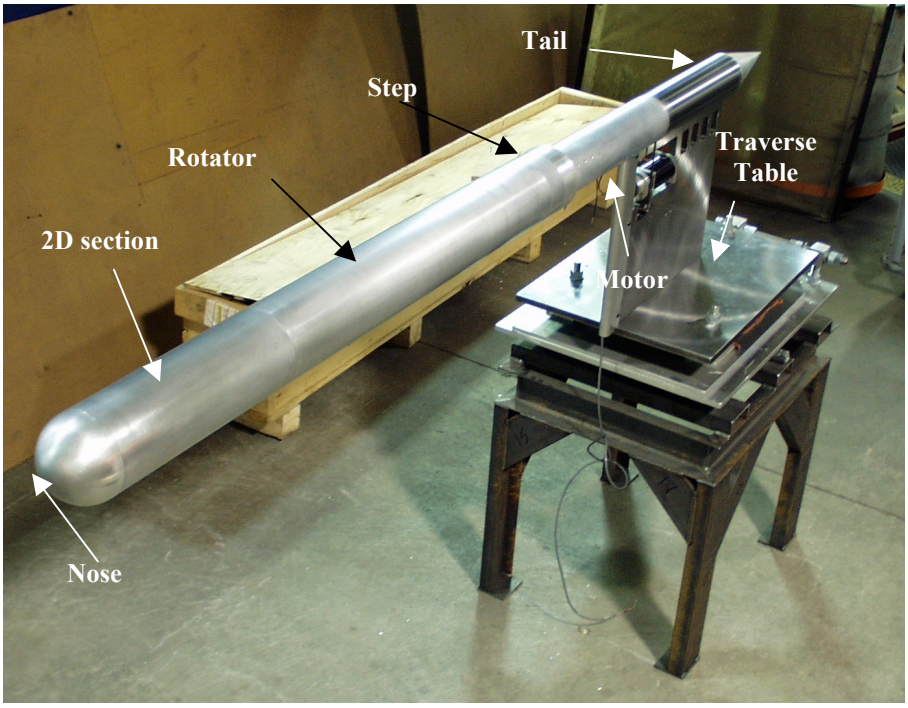

Figure 2. Axisymmetric backward-facing step model

The model measures 2.37 m in total length, 0.13 m in diameter upstream of the step, and 0.10 m in diameter downstream of the step. The step height (h) is 12 mm. The majority of the model is constructed out of aluminum with only a few steel pieces used for added strength and rigidity. Figure 3 shows a side view of the overall design of the model and the labels for various components including the nose, 2D section, rotator, step, motor/support, and tail modules. A spherical nose placed at the front of the model provided a smooth transition for the flow over the model and the conical tail prevented an abrupt transition at the aft end. The model was supported by a center steel shaft that runs the entire length of the model. Downstream of the nose is the 2D section module, measuring 0.35 m in length. This region allowed the flow to settle into a 2D boundary layer after transitioning over the nose. In addition, at the upstream end of the 2D section, sandpaper was used to trip the boundary layer and force a turbulent 2D/3D boundary layer at separation. Inside the model, a drive shaft, connected to a 1/15 hp motor, rotated the 0.75 m long rotator section upstream of the step to introduce three-dimensionality into the boundary layer as shown in Fig. 4. Without rotation, the boundary layer is 2D. Since both 2D and 3D boundary layers can develop along the surface, a comparison between the two cases within the same geometry can be made. Approximately 0.49 m or 38.4 step heights (8.3 x_r) downstream of the step is a steel motor/support module, which housed the pulley for the electric motor and provided the stability necessary to connect the model to the support stand as shown in Figs. 2 and 3.

All instrumentation was stored inside the model. Downstream of the step in the step module, the model was instrumented with 56 static pressure taps. The static pressure taps were positioned in four arrays on the top, sides, and bottom of the model and were used to characterize the mean flow surrounding the model and to align the model parallel to the free stream in the wind tunnel.

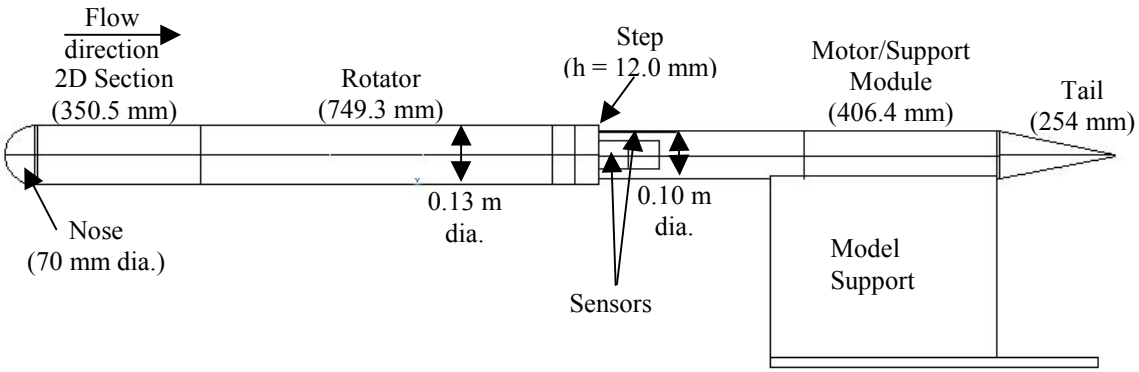

Figure 3. Side view of the axisymmetric backward-facing step

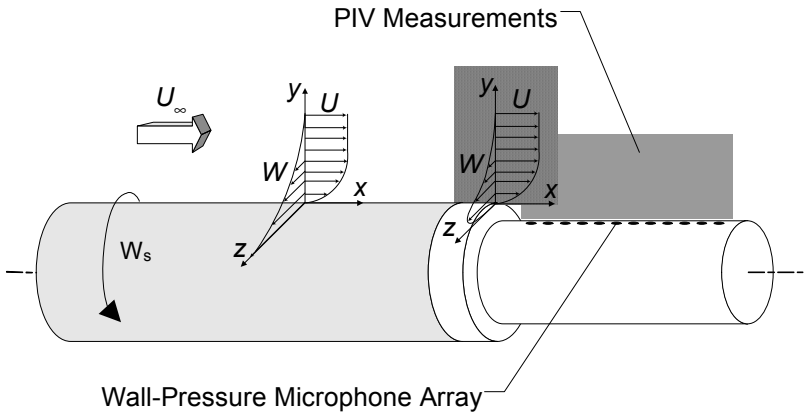

Figure 4. Schematic of boundary layer profile prior to separation

Planar PIV was used to measure the two velocity-field components over a plane parallel to the x & y axes and located along the centerline of the model, as shown in Fig. 4. The PIV system used consisted of two 1018x1008 pixel CCD cameras and two Nd: YAG lasers. The system was operated utilizing acquisition code written by NASA Glenn Research Center's Mark Wernet[12]. Due to the length of the separation zone, the field of view had to be divided into two overlapping regions: one upstream and the other downstream of reattachment. The reattachment point was captured within the second region. Nonetheless, the two views have been merged to form one complete field of view. Merging the corresponding PIV images was completed before processing the vector fields. Prior to merging the PIV images, a piecewise bilinear dewarping technique was employed to remove perspective and optical distortions. This technique of "straightening" the image was developed for Doppler Global Velocimetry by Meyers.[13]

Once merged, the PIV images were processed using Mark Wernet's PIVPROC processing code[14] and bad vectors were removed based on Chauvenet's criterion[15]. The images were processed using a multi-pass correlation technique with 50% overlap for enhanced spatial resolution and an initial 64 x 64 pixel integration box followed by a 32 x 32 pixel integration box for the second pass. This resulted in a vector spacing of 0.92 mm. Overall, the vector field map covered 101.6 mm (8.44 h) in the streamwise direction and 45.6 mm (3.8 h) in the normal direction. A total of 1500 image pairs were acquired for each of the five flow conditions tested. The free stream velocities (U_∞) for the flow conditions were 7.4, 10, 18, 23, and 40 m/s, thus resulting in a Reynolds number test range based on step height of 5900-33000. PIV data were acquired for the 2D boundary layer at all five speeds and for the 3D boundary layer at 7.4 m/s and 10 m/s only. The corresponding ratio of the cross-flow velocity of the rotator surface to freestream velocity (W_s/U_∞) for the 10 m/s case was 0.23 and 0.48. The 3D boundary layer case was measured using planar PIV. A list of the 2D and 3D cases is shown in Table 1 along with their respective Reynolds numbers based on step height (Re_h) and momentum thickness (Re_θ), reattachment distances divided by step height (x_r/h), and momentum thicknesses divided by step height (θ/h). The following Results and Discussion section focuses only on

the U_∞ = 10-40 m/s 2D cases and the W_s/U_∞ = 0.48 3D case in effort to show trends in the data while limiting the amount of data presented.

Table 1. Experimental parameters used

U_∞	Re_h	x_r/h	W_s/U_∞	Re_θ	θ/h
7.4 m/s	5980	4.28	0	889	0.149
10 m/s	8081	4.48	0	1237	0.153
18 m/s	14547	4.81	0	1751	0.122
23 m/s	18588	4.96	0	1979	0.107
40 m/s	32327	4.97	0	3280	0.104
10 m/s	8081	4.26	0.48	1558	0.196

III. Results and Discussion

The following section contains an analysis of the data collected from the PIV measurements in the separating/reattaching region downstream of the axisymmetric backward-facing step. The analysis looks at the effect of Reynolds number on the flow field downstream of a two-dimensional separating boundary layer and compares the flow field data downstream of both a two- and three-dimensional separating boundary layer condition. Preliminary measurements provide a generalized characterization of the flow field surrounding the BFS and detail the state of the boundary layer prior to separation. The technique of "forward flow probability" is described and used to determine the reattachment length for all Reynolds numbers. Mean velocity field vectors and streamlines are presented to give a spatial view of the average flow field surrounding the axisymmetric BFS. Finally, root-mean-squared (rms) and Reynolds stress statistics outline regions of fluctuating velocity in the flow field.

A. Preliminary Measurements

Preliminary measurements were made prior to acquiring the PIV data. Static pressure taps connected to a pressure transducer via a Scanivalve were used to measure the mean pressure distribution in four different azimuthal planes. These mean pressure profiles were used to align the axisymmetric BFS model within the wind tunnel and to characterize the mean-flow state surrounding the model. Additionally, boundary layer velocity profiles were acquired using X-wire anemometry approximately x = -0.083h upstream of the separating edge. These profiles provided detail regarding the state of the boundary layer and the strength of the cross-flow at separation.

The mean pressure distribution, acquired at Re_h = 8081 downstream of the axisymmetric backward-facing step using static pressure taps, is shown in Fig. 5. Both the 2D and 3D cases are displayed. The mean pressure distribution shows a classical backward-facing step pressure profile with a reattachment location of x_r = 4.48h for the 2D and x_r = 4.26h for the 3D case. The reattachment distances, as explained in the next section, were determined by calculating the "forward flow probability" near the wall from the measured PIV data. Immediately downstream of the step, the pressure distribution decreases until about $0.5x_r$ where the pressure begins to recover, reaching a peak slightly downstream of x_r. The mean pressure distribution then drops slightly as the shear layer settles back into a boundary layer. Note the mean pressure profiles are similar for both the 2D and 3D cases.

Boundary layer profiles were acquired using X-wire anemometry in order to characterize the state of the boundary layer and to measure the strength of the cross-flow at separation. Note that the size of the X-wire limited the minimum distance above the wall and therefore, it was not possible to capture the W component decreasing to zero as the wall was approached. Figures 6a-d show the mean and rms boundary layer profiles for W_s/U_∞ = 0, 0.23, and 0.48 flow cases, where U_∞ = 10 m/s. Graphs 6a and 6b present the mean velocity profiles for U/U_∞ and W/U_∞, located on the abscissa with y/δ_{99} along the ordinate. The U (capital letters denote mean values and lower case letters represent fluctuating quantities) component velocity profiles show no difference between the three flow cases at separation. However in Fig. 6b, the three-dimensionality is evident. The maximum cross-flow component at separation for the two 3D cases is W/U_∞ = 0.03 and 0.065 for the W_s/U_∞ = 0.23 and 0.48 cases, respectively. These values reflect a weak three-dimensionality, which is attributed to the relaxation that occurs over the 0.1 m distance between the rotating and separation edge. During this distance, the boundary layer begins to relax and return to a 2D boundary layer state. Since the cross-flow component at separation is weak, planar PIV could be effectively used to quantitatively measure the effect of the 3D separating boundary layer on the streamwise and normal velocity field components downstream of separation without concern about the effect of out-of-plane particle displacement.

Finally, Figs. 6c and 6d provide the streamwise and spanwise rms profiles for the W_s/U_∞ = 0, 0.23, and 0.48 flow cases. The u_{rms}/U_∞ and the w_{rms}/U_∞ are shown on the abscissa with the y/δ_{99} located on the ordinate. There is a noticeable increase in energy that can be seen in both the u_{rms} and w_{rms} plots, especially for the W_s/U_∞ = 0.48 case. Thus, the planar PIV data from the W_s/U_∞ = 0.48 case is presented in this paper since this case exhibits the highest level of three-dimensionality at the step edge.

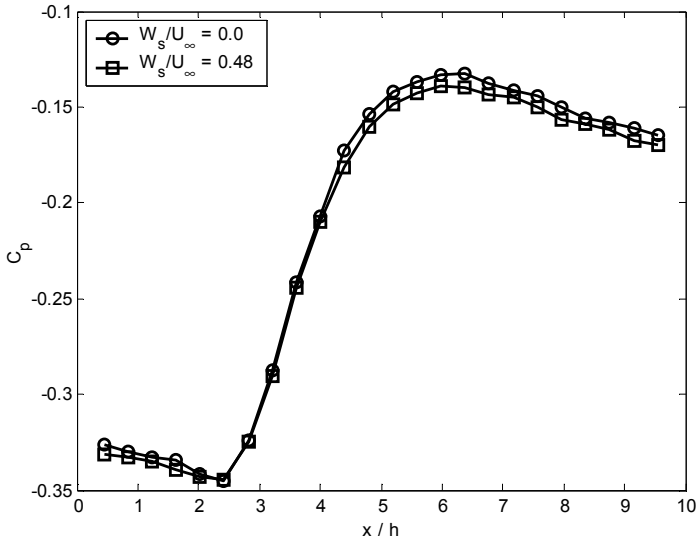

Figure 5. Mean pressure distribution for both 2D and 3D cases

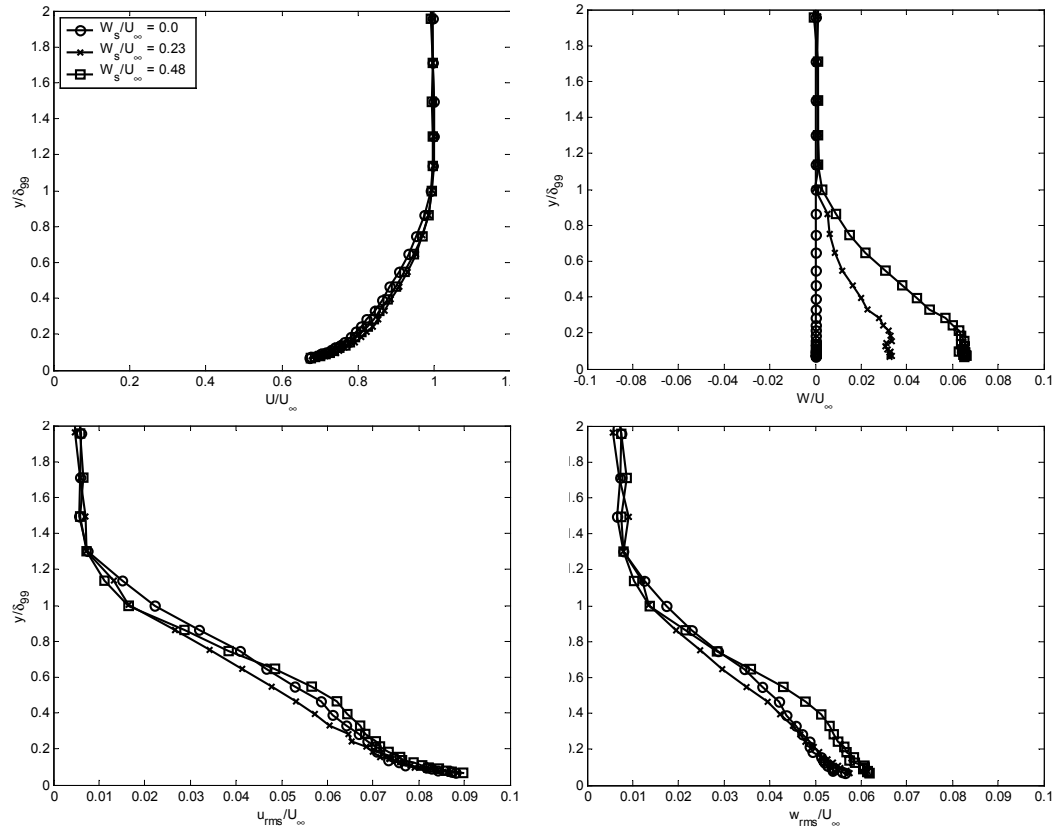

Figure 6. Mean and rms boundary layer profiles for W_s/U_∞ = 0 (o), 0.23 (x), and 0.48 ( ) cases

B. Reattachment Length

The reattachment distances listed in Table 1 were determined using forward flow probability (FFP) as demonstrated by Spazzini *et al.*[9], Eaton[16], Westphal and Johnston,[17] and Tihon *et al*[18]. FFP is the fraction of the time that the flow is in the forward direction. In each image, the direction of the flow measured at y/h = 0.026 (y = 0.3 mm) is recorded and the FPP is determined as the number of images for which the velocity is positive divided by the total number of images. The results are presented as percentages along the ordinate as shown in Fig. 7, with the normalized streamwise distance along the abscissa. A 0% FFP means the flow at that particular x/h position is always moving toward the step; whereas, 100% FFP indicates that the flow is always in the downstream direction. The reattachment distance is located at the streamwise position where the FFP = 50%. Due to slight scatter in the data, a seventh-order polynomial fit was used to estimate the function of the FFP versus streamwise distance.

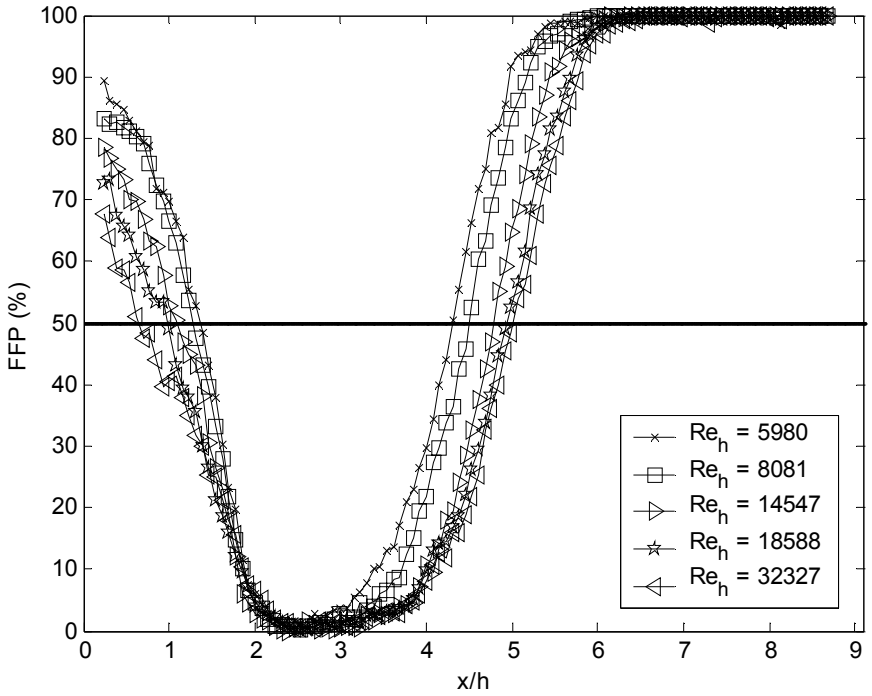

Figure 7. Streamwise distribution for the forward flow probability for all five Reynolds number based on step height 2D cases

In Fig. 7, data for the 2D case at all Reynolds numbers are plotted. There are two streamwise positions where the FFP = 50%. Depending on the Reynolds number, the first streamwise position is between x/h = 1 – 1.5 and the second position is roughly between x/h = 4 – 5. The first position gives the location of the secondary separation point close to the step, which separates the secondary and primary re-circulating regions. The second FFP = 50% position is the point of reattachment of the shear layer. The five cases plotted in Fig. 7 show that increasing the Reynolds number results in a longer primary reattachment length and a shorter secondary separation point. Similar results, within 3.6%, were found in the same geometry by Li and Naguib[7] from wall-shear measurements using an oscillating hotwire at y/h = 0.008. Spazzini *et al.*[9] also report the same trend for the Re_h range 3500 through 16000. Li and Naguib[7] attribute this trend to the variation in the boundary layer thickness. This reasoning is supported by the earlier observations of Eaton and Johnston[2] and Adams and Johnston[8], both of whom found that x_r increased as the boundary layer thickness decreased. Since in this study the Reynolds number increases by increasing the freestream velocity, the boundary layer thickness should decrease as Re is increased. Referring to Table 1 and Fig. 8, this is seen to be in fact the case for U_∞ of 10 m/s (Re_h = 8081) and higher where the value of θ is found to decrease with Re_h. However, the lowest Re_h case (U_∞ = 7.4 m/s) deviates from this trend where the momentum thickness is seen to be smaller than that at Re_h = 8081. This is attributed to possible "under stimulation" of the boundary layer at the lowest freestream speed, suggesting that the boundary layer may not be sufficiently developed to a turbulent state as in the other cases.

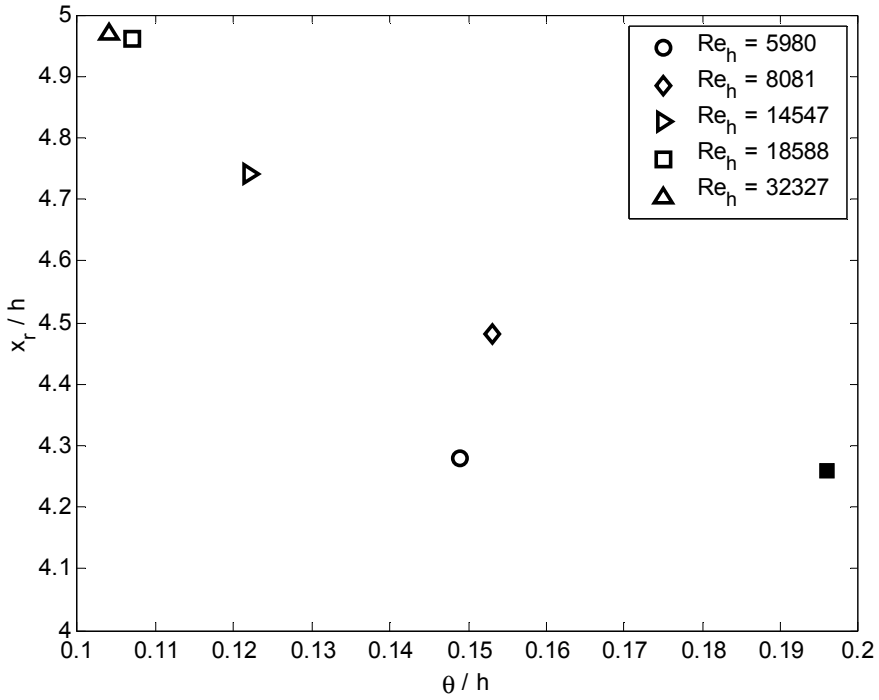

Figure 8. Normalized reattachment distance versus momentum thickness 2D cases (open symbols) and 3D case (■)

Figure 9 exhibits the FFP as a function of normalized streamwise distance for the 2D and 3D, Re_h = 8081 cases. In addition, the seventh-order polynomial fit is plotted in Fig. 8 for each case. In terms of the 3D case, because only the upstream PIV image was processed for this case, the data do not extend to reattachment. Therefore, x_r for the 3D case is estimated from the polynomial fit. Table 1 shows that the momentum thickness (θ) for the 3D case is about 30% higher than the 2D case at the same Re_h. The measured reattachment distance for the 2D case is x_r = 4.48h while x_r for the 3D case is x_r = 4.26h. The x_r for the 3D case is roughly 5% shorter than the 2D x_r. As the momentum thickness of the boundary layer is increased, the reattachment length is reduced as shown in Fig. 8. This suggests that the observed reduction in x_r because of 3D effects may merely be a reflection of the corresponding change in boundary layer characteristics at separation rather than the existence of a different fluid dynamical phenomenon because of the cross-flow shear. This seems like a reasonable interpretation for the current data where the cross-flow component is substantially weaker than the streamwise component. It is unlikely, however, that this will be the case for boundary layers with equally-strong, or dominant, cross-flow component. Finally, while a difference was seen in the primary reattachment length, no change was seen in the secondary separation point between the two cases.

Figure 10 shows the reattachment distances as a function of Reynolds number for both the 2D and 3D cases. As the Reynolds number increases in the 2D cases, x_r increases; although, the data suggests that the reattachment distance plateaus at some "critical" Reynolds number as shown by the two highest Re having similar x_r values. Nonetheless, further information is needed to make such a conclusion. In terms of the 2D versus 3D cases, the reattachment distance for the W_s/U_∞ = 0.48 case is shorter than the x_r distance for the W_s/U_∞ = 0.00 case as discussed above.

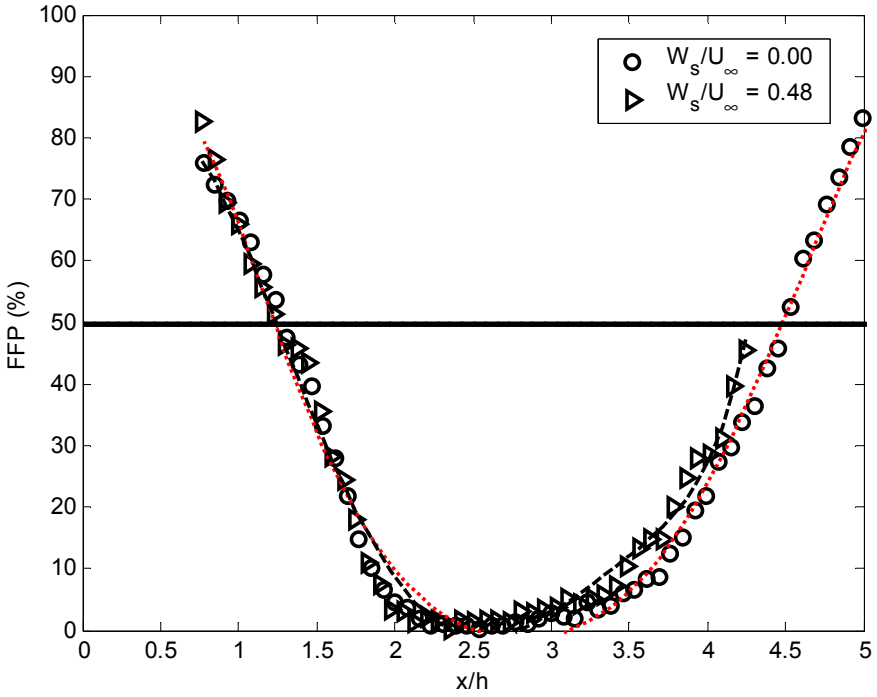

Figure 9. Streamwise distribution for the forward flow probability for the 2D and 3D cases

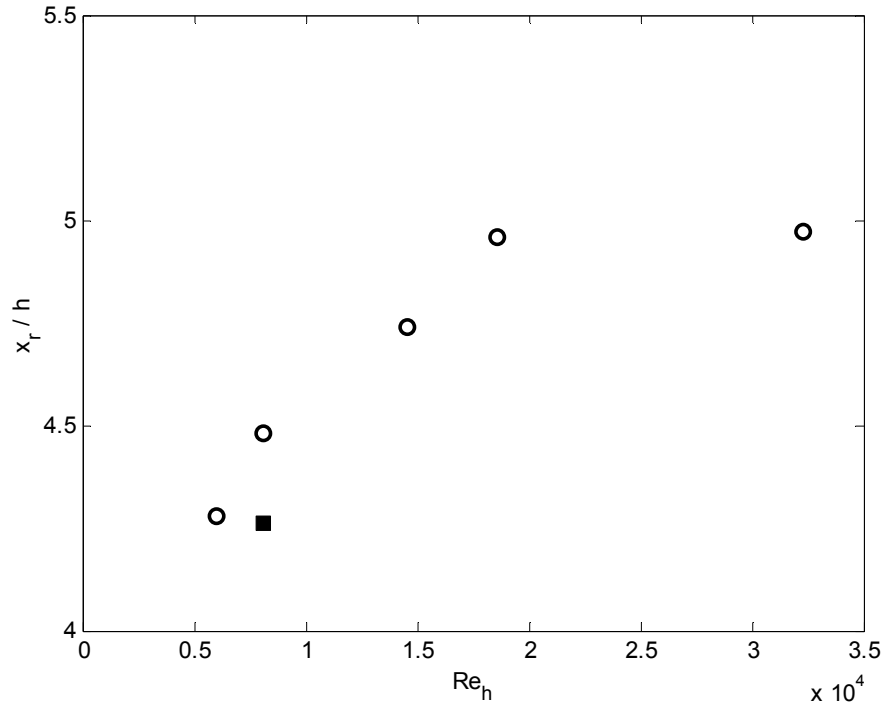

Figure 10. Reynolds number based on step height versus reattachment distance for all five 2D cases (O) and the 3D case (■)

C. Mean Velocity Distributions

The mean velocity vector fields and streamlines above the surface downstream of the axisymmetric backward-facing step are shown in Figs. 11a-d for four of the five 2D cases, spanning Re_h = 8000-33000. The streamwise distance, x/h, is along the abscissa and the distance normal to the wall, y/h, is represented along the ordinate axis. The vector fields show a classical backward-facing step mean velocity field. The boundary layer separates at the edge of the step forming a shear layer that reattaches a distance downstream of the step. The streamlines curve towards the wall with increasing x until the shear layer reattaches at x_r. Beneath the shear layer there is a clockwise recirculation zone located near the wall that stretches from x/h ~ 1.1 - x_r depending on Reynolds number. The reattachment point was captured for all four Reynolds numbers and as seen in the FFP plots earlier (Fig. 7), the reattachment length increases with increasing Reynolds number. Near the step, within the x/h = 0-1.1h region, the streamlines indicate a secondary recirculation zone, which is a characteristic feature in BFS flows. Scarano and Riethemuller[11] along with Kostas et al.[10] were also able to capture the secondary recirculation zone in their PIV studies of a planar BFS. As observed in the FFP analysis as well as recorded in studies by Spazzini *et al.*[9] and Li and Naguib[7], there is a reduction in the size of the secondary re-circulating region with increasing Reynolds number. Beyond reattachment, the shear layer forms a reattached boundary layer as shown in Figs. 11a-d for all Reynolds numbers.

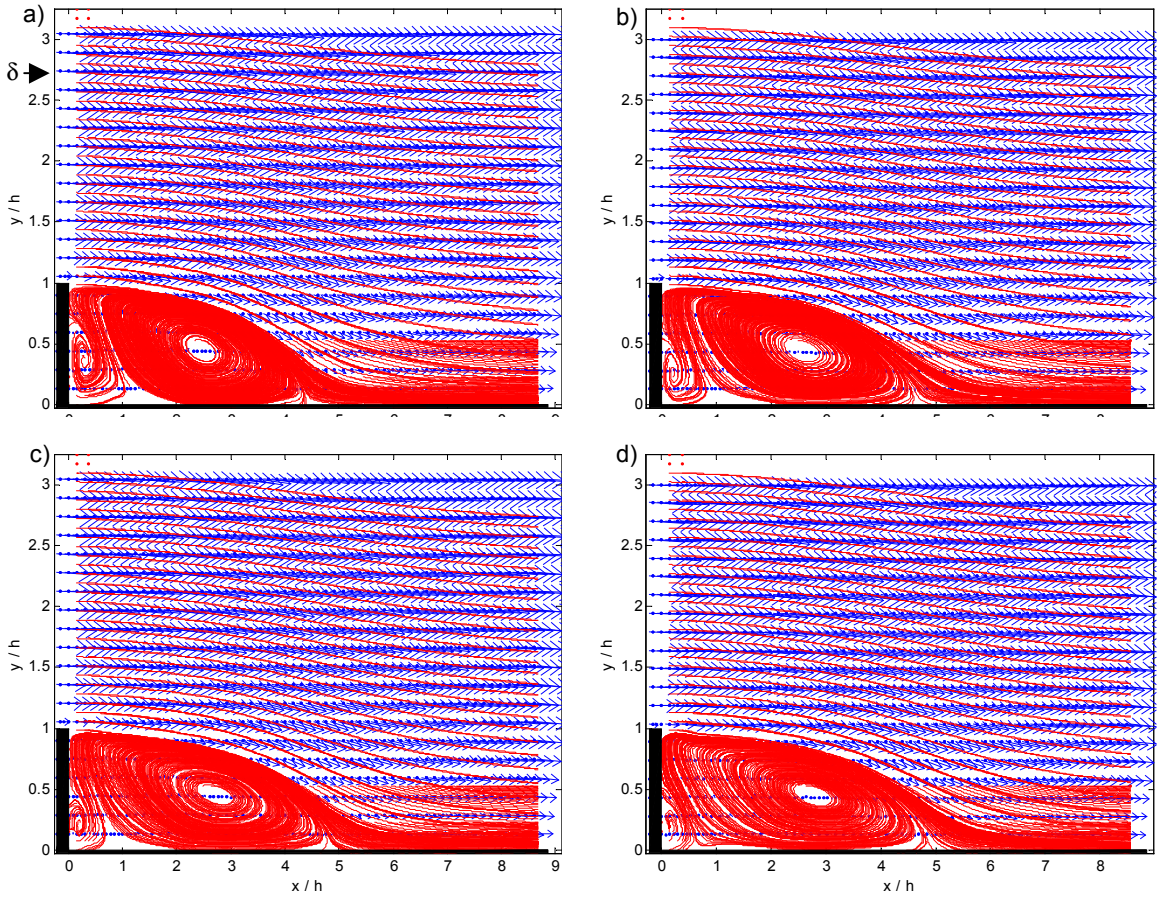

Figure 11. Mean velocity profiles for Re_h = a) 8081, b) 14547, c) 18588, and d) 32327

Figure 12a-b compares the mean velocity vector fields and streamlines above the surface in the axisymmetric backward-facing step from the 2D and 3D cases. Both of these cases have a Re_h = 8081, with a Re_θ = 1237 and 1558 for the 2D and 3D cases, respectively. The two vector fields are quite similar with no evident differences caused by the three dimensionality. The 5% difference in x_r found from FFP analysis would be difficult to depict from visual observation of the vector field and streamlines.

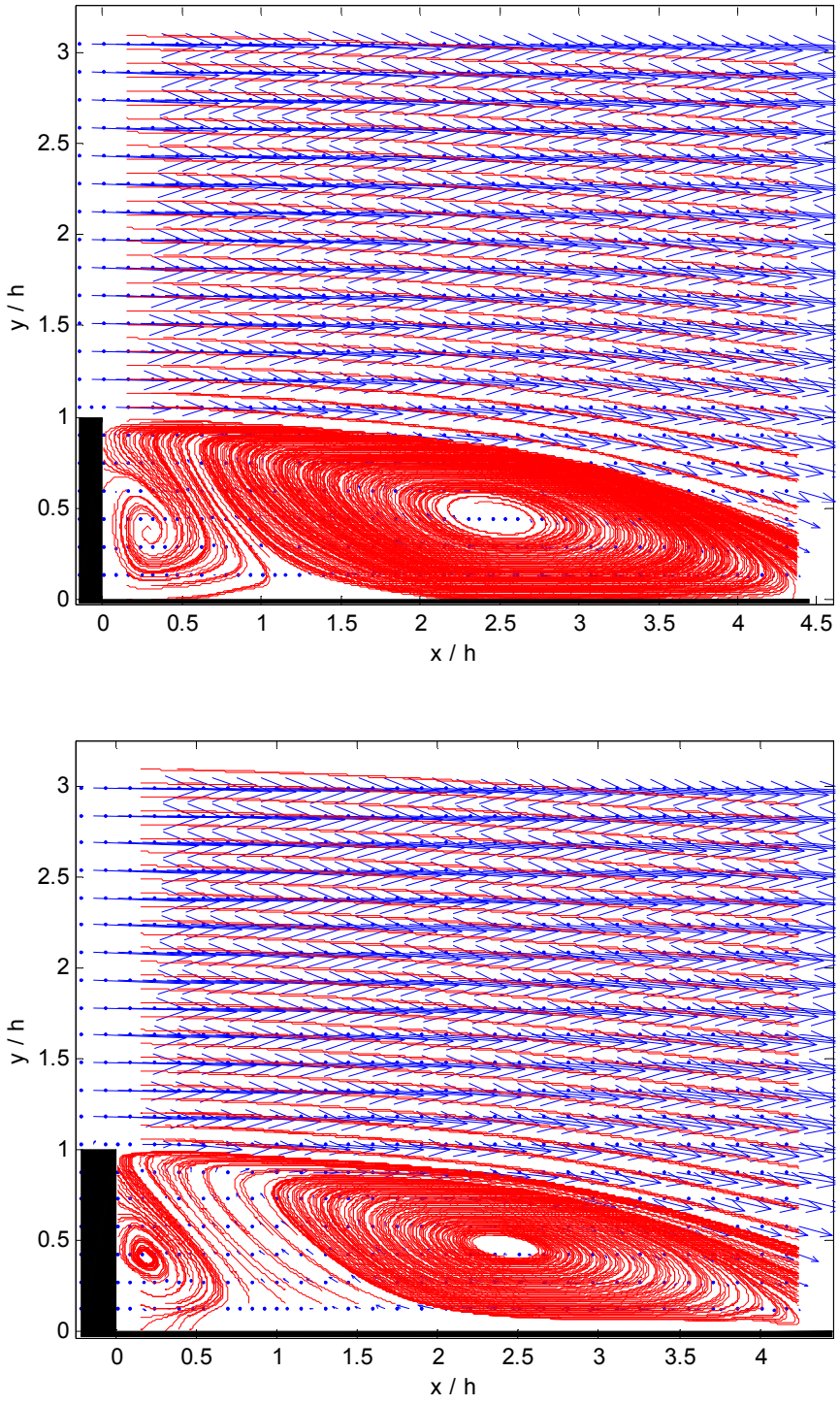

Figure 12. Mean velocity vector profiles with streamlines for the 2D case $Re_h = 8081$, $W_s/U_\infty = 0$ (top) and the 3D case $Re_h = 8081$, $W_s/U_\infty = 0.48$ (bottom)

To take a closer look at the mean-velocity-field characteristics, mean velocity profiles extracted from the planar PIV data at six different x/h positions are shown in Fig. 13 for both the 2D and 3D cases. The six positions are

located at x/h = 0.85, 2.08 3.54, 4.23, 6.07, and 8.06. Along the abscissa the normalized velocity is presented as U/U_∞ and along the ordinate the distance normal to the wall is given as y/h for all six x/h positions. The top three plots have both the 2D cases for Re_h = 8081 and 32327 and the 3D case for Re_h = 8081 and W_s/U_∞ = 0.48. In general, the top three plots are located downstream of separation and upstream of the reattachment point. These three plots show the reverse flow below the step height, the shear layer region, and the relatively unchanged boundary layer-like profile starting around y/h > 1. The fourth plot, x/h = 4.22 is near reattachment and at this point slightly more reverse flow is seen in the Re_h = 32327 case than the Re_h = 8081 case since the former case reattaches 0.49h farther downstream. The last two velocity-profile plots are located downstream of reattachment. It is in this region that the flow reattaches and begins to relax towards an equilibrium boundary layer state.

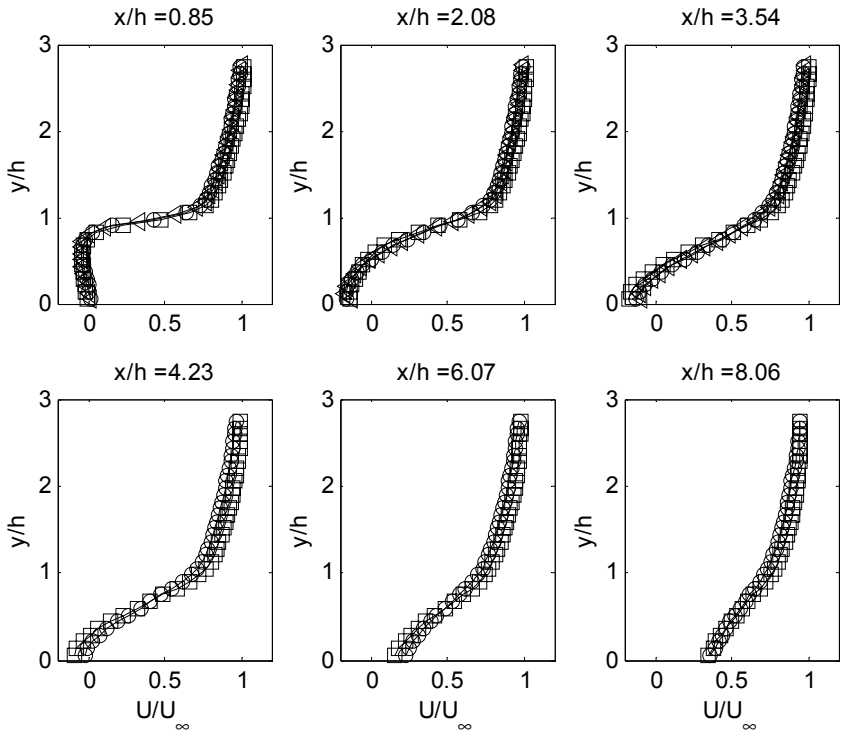

Figure 13. Mean streamwise velocity profiles at selected streamwise locations: (O)Re_h = 8081, W_s/U_∞ = 0.00, ( ) Re_h = 32327, W_s/U_∞ = 0.00, (◁) Re_h = 8081, W_s/U_∞ = 0.48

To elaborate further, starting with the x/h = 0.85 plot located downstream of the step, the three profiles show the reverse flow beneath the step height, y/h = 1. Around y/h = 1, the velocity changes rapidly over a very short y distance, indicating this is the shear layer region. Near the step, the shear layer is thin causing a large velocity gradient. At y/h > 1, the velocity profile takes on profile similar to that of the boundary layer upstream (not shown here) away from the near-wall region. This gives indication that the boundary layer once it separates remains unaffected except in the region close to the wall. In their study of a single-stream shear layer, Morris and Foss[19] introduced the idea that the initial shear layer instability originates only from within the near-wall region of the boundary layer, forming a "sub-shear layer" immediately downstream of separation. The rest of the boundary layer remains intact until farther downstream when the sub-shear layer grows sufficiently to affect the full width of the shear layer. Morris and Foss[19] stated that the mean profiles are identical for $y/\theta > 2$ for a streamwise distance between $0 < x/\theta < 29$. The first four plots in Fig. 13 have x/θ equal to 5.5, 13.6, 23.1, and 27.6 for Re_h = 8081. Further discussion on the point will be given in Section D of the Results and Discussion. Farther downstream, the steep velocity gradient in the shear layer region relaxes and the shear layer spreads out. This can be seen in the next two plots, x/h = 2.08 and 3.54, where the velocity gradient around y/h = 1 is not as steep. In addition, the vertical height of the reverse flow region becomes smaller as the shear layer curves toward the wall. At x/h = 4.23, the reverse flow region is almost non-existent as the shear layer nears the reattachment point.

Comparing the 2D and 3D, Re_h = 8081, cases there is a slight difference between the mean velocity profiles. The same trend is more noticeable between the two 2D cases over the range y/h = 1- 3. The differences here may be due to scaling. More specifically, since the profiles are extracted at the same x/h positions, the shear layer development relative to the reattachment distance is different for each case at the same x/h. By selecting streamwise positions based on x/x_r, the profiles may collapse.

D. Fluctuating Velocity Distributions

Figures 14-17 show the longitudinal (u_{rms}) and vertical (v_{rms}) turbulent fluctuations for the 2D and 3D cases. Each figure is a flooded gray-shade contour map with the streamwise distance, x/h, along the abscissa and the distance normal to the wall, y/h, along the ordinate. The color bar on the side of the contour plot indicates the magnitude of the particular turbulent rms velocity normalized by U_∞. For all plots in Figs. 14-17, the peak root-mean-squared values are located within the separating shear layer, with the highest peak along the center of the shear layer near the separation edge. The 2D case data presented in Figs. 14-15 compare well, qualitatively, with Scarano and Riethmuller[11] in their PIV study of a planar backward-facing step. In addition, the general behavior observed is consistent with the findings of Castro and Haque[4] as well as Ruderich and Fernholz[20] in their investigations of a fence-with-splitter-plate flow. Both studies were able to use the maximum loci in the turbulent intensity plots to determine the center of the separating shear layer. Qualitatively, the rms magnitudes in the current study are higher than in Scarano and Riethmuller's[11] study. In particular, the u_{rms} and v_{rms} values are almost double the values found by those authors. It is interesting to note that, in contrast to a free shear layer which spreads gradually and smoothly with increasing x, the reattaching shear layer initially diverges smoothly until approximately x/h ~ 2 when a "sudden" divergence occurs and the shear layer grows to a thickness approximately equal to the step height.

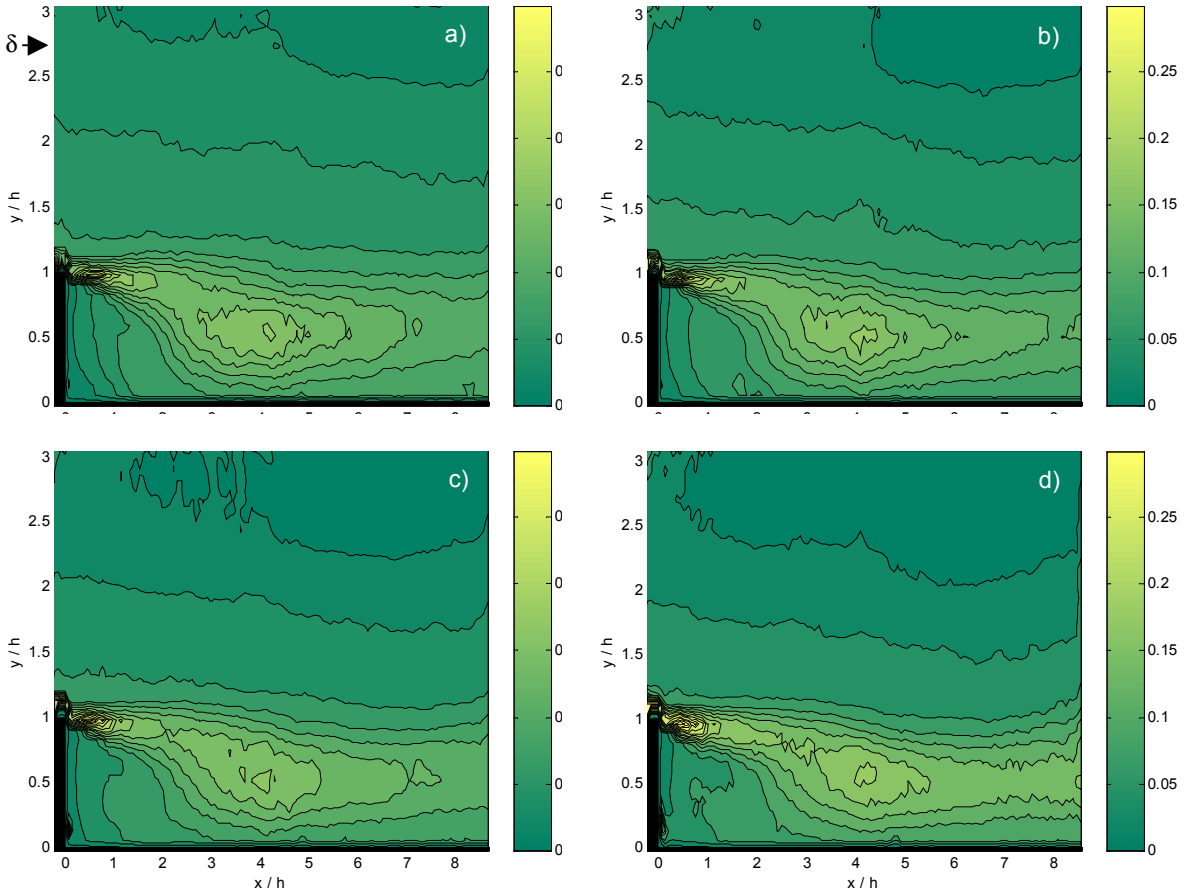

Figure 14. Gray-scale contour maps of u_{rms}/U_∞ for the 2D separating flow at Re_h = a) 8081, b) 14547, c) 18588, and d) 32327

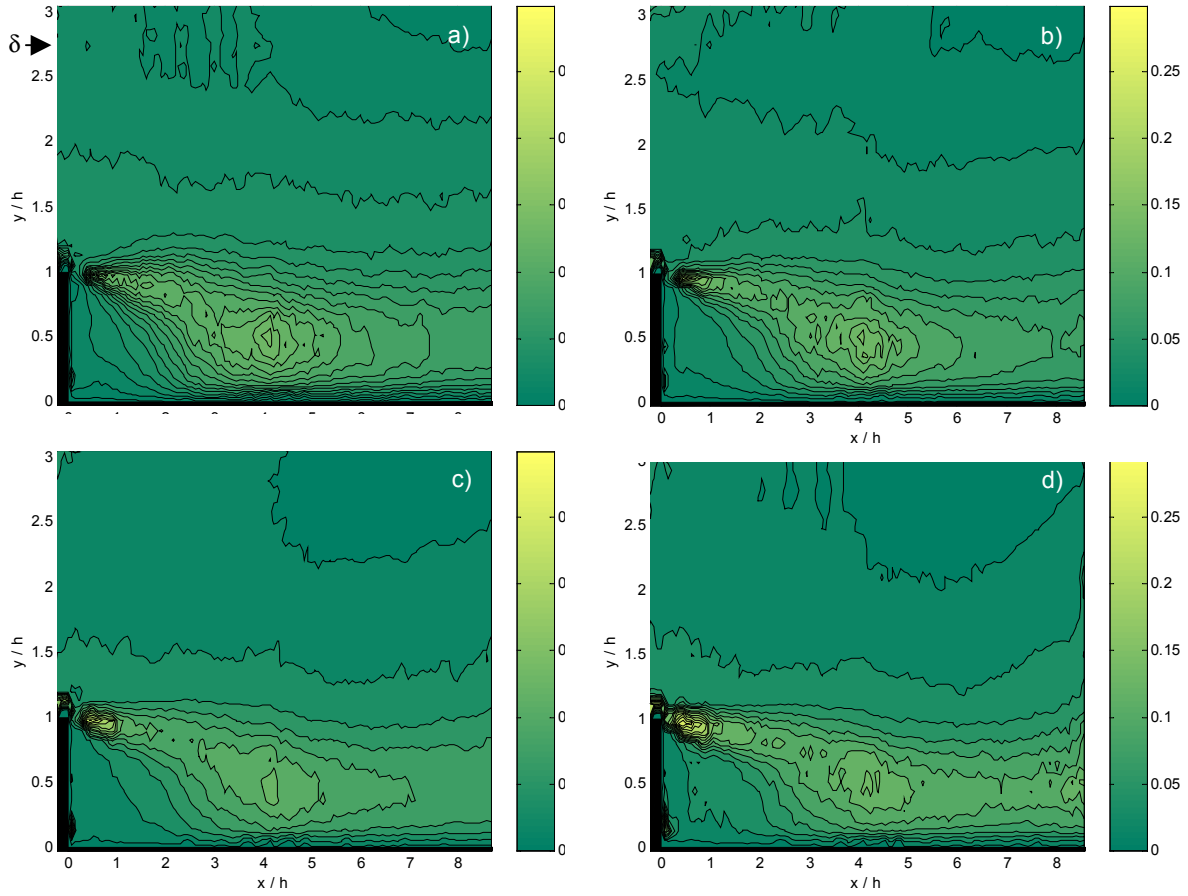

Figure 15. Grey-scale contour maps of v_{rms}/U_∞ for the 2D separating flow at Re_h = a) 8081, b) 14547, c) 18588, and d) 32327

In Fig. 14a-d, the u_{rms} contour maps outline the shear layer and the boundary layer distinctly for the four Reynolds number cases, spanning 8000 to 33000. Within the separating sub-shear layer (the thin region of high shear near y/h = 1 and immediately downstream of the step), the u_{rms} values change dramatically over a short x distance due to the high shear in the region. Above the sub-shear layer, starting around y/h = 1.25, the u_{rms} values decrease slowly over a large streamwise distance in the downstream direction. That is, within this zone very little change is observed in the turbulence activity in the outer part of the separating boundary layer, and hence the flow structure characteristics are likely to be similar to those in the boundary layer. At the edge of the boundary layer, $\delta = 1.73h$, the u_{rms} values are less than $u_{rms}/U_\infty = 0.02$ as the boundary layer merges with the free stream. In Figs. 14a-d, distinct u_{rms} bands can be seen at the different heights in the boundary layer. These u_{rms} values decrease with increasing height in the boundary layer as expected. In addition, the u_{rms} bands show a slight curvature toward reattachment upstream of reattachment. Beyond reattachment, the bands become parallel to the wall as the shear layer transitions to a reattached boundary layer. In addition, the shear layer loses energy once the shear layer reattaches as can be seen by the reduction in u_{rms} magnitude beyond reattachment.

A point of interest is the two peaks in the u_{rms} that can be seen in the shear layer at x/h ~ 0.1-1 and 4.2. The peak closest to separation increases in magnitude with increasing Reynolds number and has a higher magnitude than the second peak. This local maximum value close to separation has also been seen by Morris and Foss[19] in their single-stream shear layer study. Morris and Foss[19] found a local maximum value located roughly at $x/\theta \sim 2$ and $y/\theta \sim 0.15$. Such a local maximum value has been observed in the literature only in laminar separating boundary layers. Hence, it appears that the present data support the findings of Morris and Foss[19], whose boundary layer was also turbulent at separation, suggesting that the sub-shear layer region is dominated by viscous effects from the near-wall at separation. Nonetheless, caution should be exercised since the region immediately downstream of the separation point is a high-shear region and the accuracy of the PIV results there may be questionable. Therefore, to check that the peak near separation is not an artifact of the PIV processing, the data near separation will be re-processed using

iterative methods, such as particle image distortion (Huand and Fidler[21]) that have been developed to remedy high-shear effects on PIV measurements. The second peak occurs slightly upstream of reattachment, x/h ~ 4.2. Scarano and Riethmuller[11] find their maximum u_{rms} value about one step height upstream of reattachment. The same trend has also been recorded in surface pressure measurement studies in planar BFS. For example, Heenan and Morrison[22] observed in their study that the maximum p_{rms} value is located approximately one step height upstream of reattachment.

The comparison between all the 2D cases shows no noticeable difference in the u_{rms} distribution. This can be seen in the u_{rms} profiles plotted in Fig. 18 for six streamwise positions. In Fig. 18, plotted in the top three graphs are the 2D and 3D cases with the bottom three plots only showing the 2D cases since the data processed thus far for the 3D case only contains information up to right before the reattachment point. Focusing on the top three plots in Fig. 18, overall the three profiles collapse throughout the shear layer and separation region, except in the peak region near separation where both the Re = 8081, 3D case and the Re = 32327, 2D case are greater in magnitude then the Re = 8081, 2D case. Also, there seems to be more streamwise fluctuations in the separating flow region above the sub-shear layer in the Re = 8081, 2D case than in the other two cases. The bottom three plots show only the 2D case profiles. These profiles almost collapse at each streamwise position shown; however, the profiles are being compared are in different development stages with respect to their reattachment distance. Thus, the profiles may collapse completely if plotted at the same x/x_r positions.

In terms of comparing the 2D case versus the 3D case, two distinct differences are evident as can be seen in Fig. 16. First, the peak close to separation has a higher magnitude in the 3D case than in the 2D case. Second, the peak is broader in the y direction and extends farther downstream in the 3D case than in the 2D case. Downstream of the local maximum value the two cases appear similar. This suggests that since the cross-flow was weak at separation, most of the three-dimensionality influence was limited to enhancing the turbulence activity in the initial development of the shear layer, but that the three-dimensionality effects died farther downstream; thus having no global influence on the separation bubble.

Gray-scale contour maps of the v_{rms} for the 2D separating flow at four different Reynolds numbers are shown in Fig. 15a-d. The contour maps have similar characteristics compared to the longitudinal turbulent intensity maps as evidenced by the higher intensity values being contained within the shear layer. In addition, v_{rms} bands can be seen located above the shear layer with slight curvature toward reattachment; although, these bands are not as defined as the u_{rms} bands. Nonetheless, the v_{rms} values decrease with increasing height within the boundary layer.

The effect of increasing Reynolds number is evident in the vertical turbulent intensity contour maps. One of the most noticeable characteristics of increasing the Reynolds number is that the magnitude of the peak value, located at x/h ~ 0.1-1 as seen in the u_{rms} contour maps, increases. The other interesting change that can be seen with changing Reynolds number is the shape of the shear layer, which changes with increasing Reynolds number. At lower Reynolds numbers such as Re = 8081, the shear layer is more spread out and the energy seems to be diffusing out into the surrounding flow; whereas, at higher Reynolds numbers such as Re = 32327, the shear layer is more streamlined.

The v_{rms} gray-scale contour plots for both the 2D and 3D cases are shown in Fig. 17a-b. The only difference between the two cases is the magnitude of the peak near separation is greater in the 3D than the 2D case. This can be easily seen in the v_{rms} profiles in Fig. 19. The energy associated with the peak seen in the 3D case near separation (x/h = 0.85) is equivalent to that seen in Re = 32327 2D case. These peaks have double the magnitude seen in the 2D, Re = 8081 case. It is interesting to note that between x/h = 0.85 and 2.08 the peak for the Re = 8081, $W_s/U_\infty = 0$ case spreads out vertically, but does not increase in magnitude; whereas, for the other two cases the peak decreases in magnitude and spreads out vertically so that at x/h = 2.08, all three profiles collapse. Moving farther downstream, at x/h = 3.54, all three profiles collapse. Even through reattachment the 2D case profiles collapse, but beyond x_r the Re = 8081 2D flow loses energy faster than the Re = 32327 2D case as shown in x/h = 6.07 and 8.06. Nonetheless, the two profiles may not collapse at these particular x/h positions because each is at a different streamwise position with respect to reattachment. As previously mentioned, if the profiles were plotted at the same x/x_r positions, then all might collapse because each would be in the same development stage with respect to reattachment.

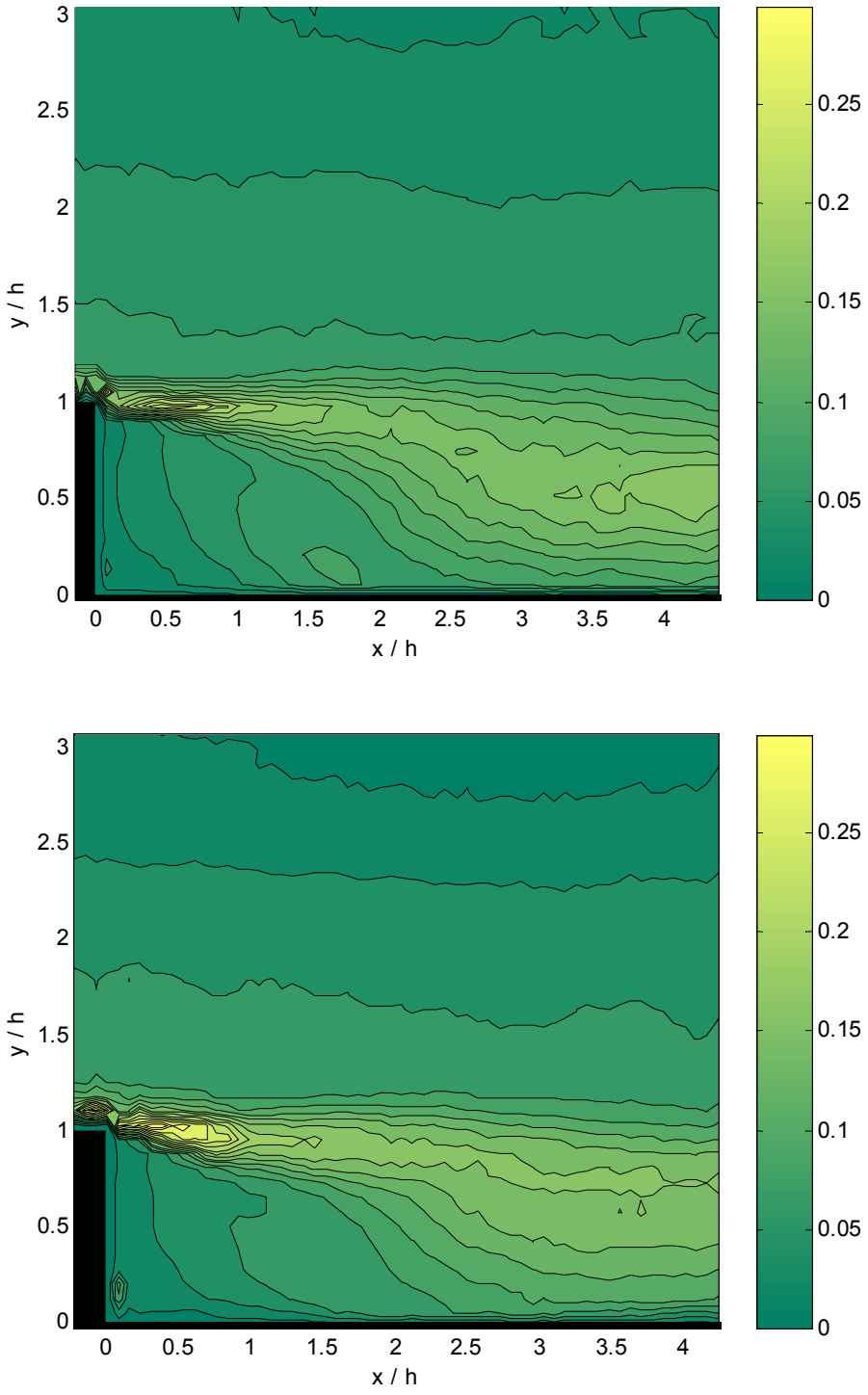

Figure 16. u_{rms}/U_∞ rms gray-scale contour maps for the 2D case $Re_h = 8081$, $W_s/U_\infty = 0$ (top) and the 3D case $Re_h = 8081$, $W_s/U_\infty = 0.48$ (bottom)

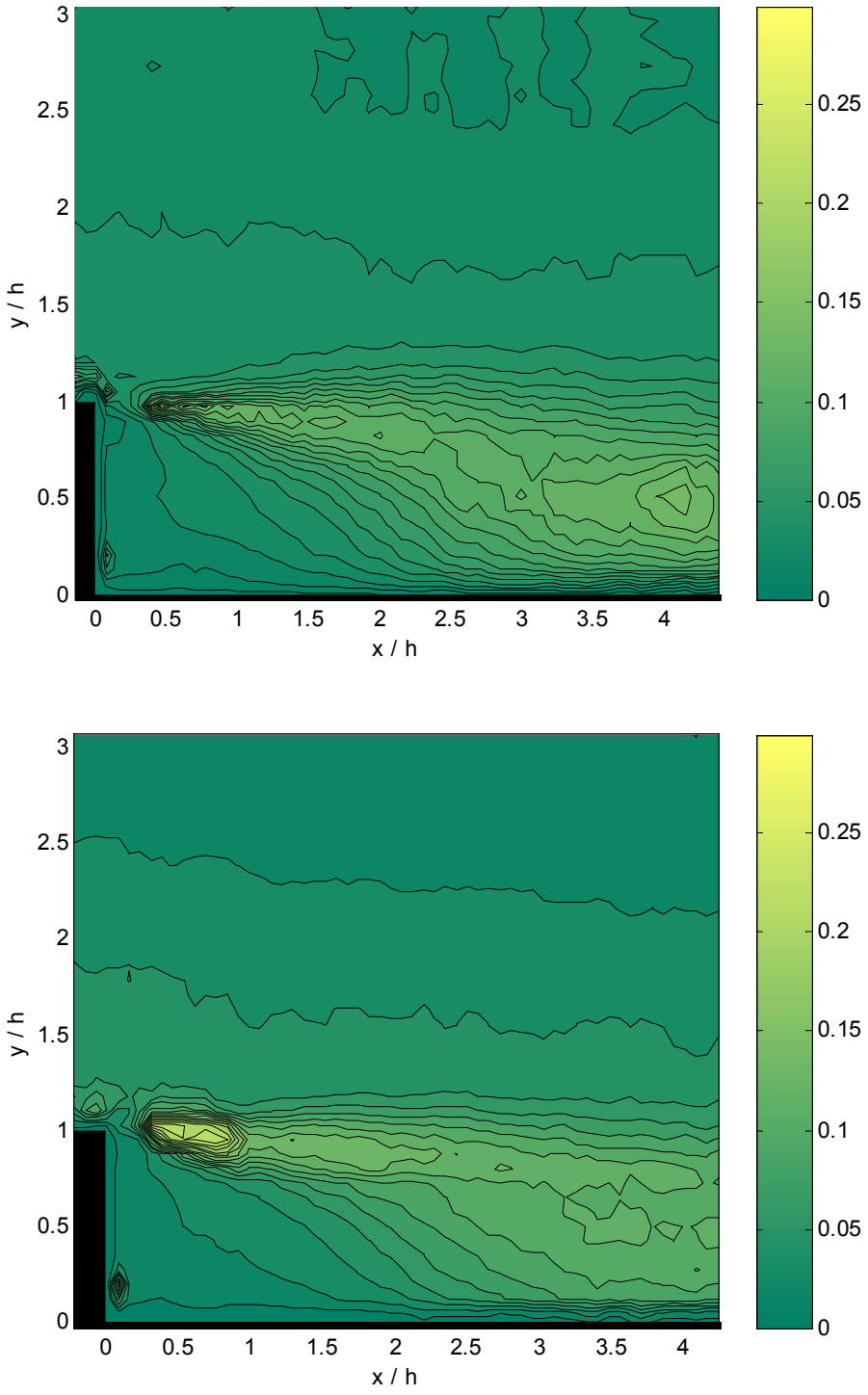

Figure 17. v_{rms}/U_∞ gray-scale contour maps for the 2D case $Re_h = 8081$, $W_s/U_\infty = 0$ (top) and the 3D case $Re_h = 8081$, $W_s/U_\infty = 0.48$ (bottom)

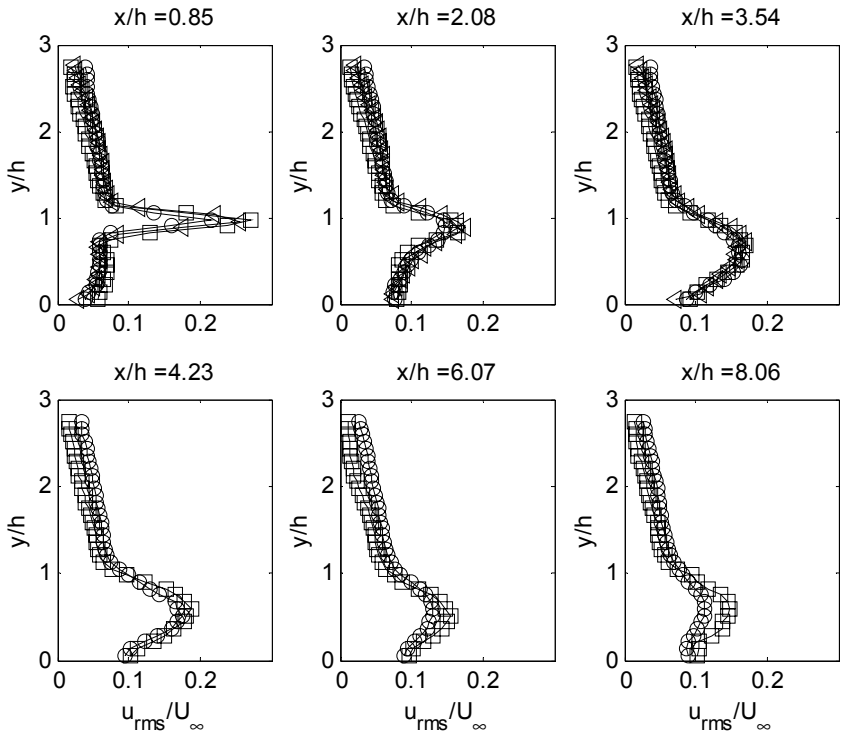

Figure 18. Streamwise velocity rms profiles: (O)Re_h = 8081, W_s/U_∞ = 0.00, ( ) Re_h = 32327, W_s/U_∞ = 0.00, (◁) Re_h = 8081, W_s/U_∞ = 0.48

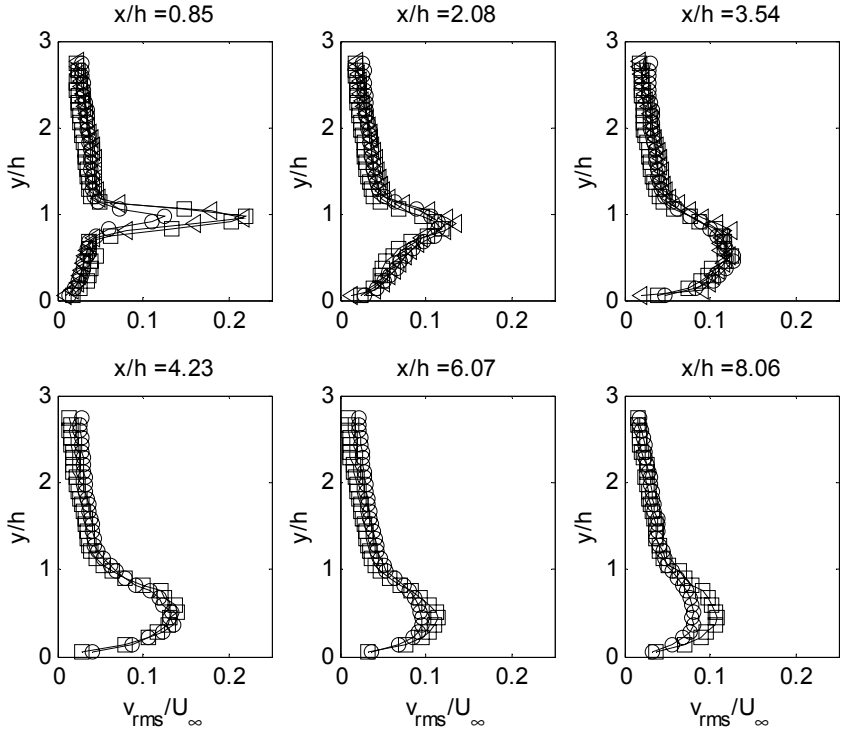

Figure 19. Normal velocity rms profiles: (O)Re_h = 8081, W_s/U_∞ = 0.00, ( ) Re_h = 32327, W_s/U_∞ = 0.00, (◁) Re_h = 8081, W_s/U_∞ = 0.48

E. Reynolds Shear Stress

Figures 20 through 22 provide the Reynolds shear stress, $-\overline{u'v'}/U_\infty^2$, information for the axisymmetric backward-facing step. Figure 20a-d contains the color contour maps for the Reynolds shear stress from the 2D cases for all four Reynolds numbers; whereas, Fig. 21a-b show the gray-scale contour maps for the Re = 8081, 2D case versus the Re = 8081, 3D case. The axes for the contour plots are the same as seen previously with the streamwise coordinate represented on the abscissa and the normal direction on the ordinate. The colorbar to the right of the map gives the magnitude of the Reynolds stress. Finally, Fig. 22 provides the individual $-\overline{u'v'}/U_\infty^2$ profiles for three cases: 1) Re = 8081 and $W_s/U_\infty = 0$, 2) Re = 32327 and $W_s/U_\infty = 0$, and 3) Re = 8081 and $W_s/U_\infty = 0.48$. In these profile plots, $-\overline{u'v'}/U_\infty^2$ is plotted along the abscissa and the ordinate shows the normal direction normalized by the step height.

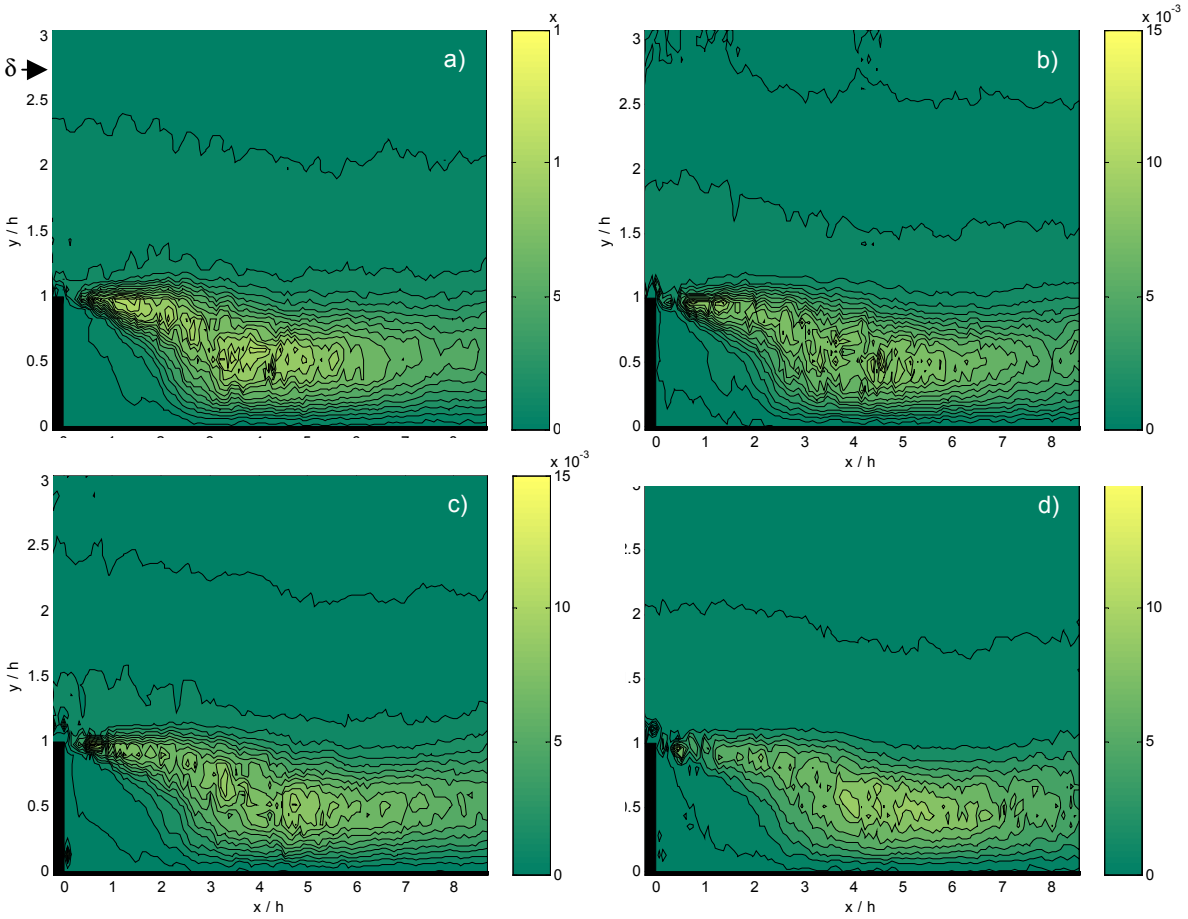

Figure 20. Gray-scale contour maps of $-\overline{u'v'}/U_\infty^2$ for the 2D separating flow at Re_h = a) 8081, b) 14547, c) 18588, and d) 32327

Starting with the gray-scale contour maps in Fig. 20, it is interesting to point out that the magnitude of the Reynolds shear stress decreases as the Reynolds number is increased. This may be explained by looking at the scaling used in the contour maps. The Reynolds stress values in the contour maps are all normalized by U_∞^2. However, Morris and Foss[19] suggested that the Reynolds stresses a single-stream shear layer should scale with the separating boundary-layer friction velocity (i.e., wall-shear stress), at least close to separation. Thus, since the skin-friction coefficient of the boundary layer (which is essentially equal to the square of the friction velocity divided by U_∞^2) decreases with increasing Reynolds number, then the ratio of friction velocity to freestream velocity decreases with Re_h as well (when Re_h is increased by increasing U_∞ as done here). This means that the freestream velocity changes faster than the friction velocity with increasing Re_h. Thus, if $-\overline{u'v'}/u_\tau^2$ (u_τ is the friction velocity) does remain invariant with Reynolds number as hypothesized by Morris and Foss, then $-\overline{u'v'}/U_\infty^2$ at a higher free stream

velocity will be lower than $-\overline{u'v'}/U_\infty^2$ at a lower freestream. This decrease of $-\overline{u'v'}/U_\infty^2$ with increasing Re may provide an explanation for the increase in x_r for higher Re cases. More specifically, the lower Reynolds stress values result in lower rate of turbulent diffusion of momentum in the wall normal direction, and hence lower spread rate of the shear layer as well as longer reattachment length.

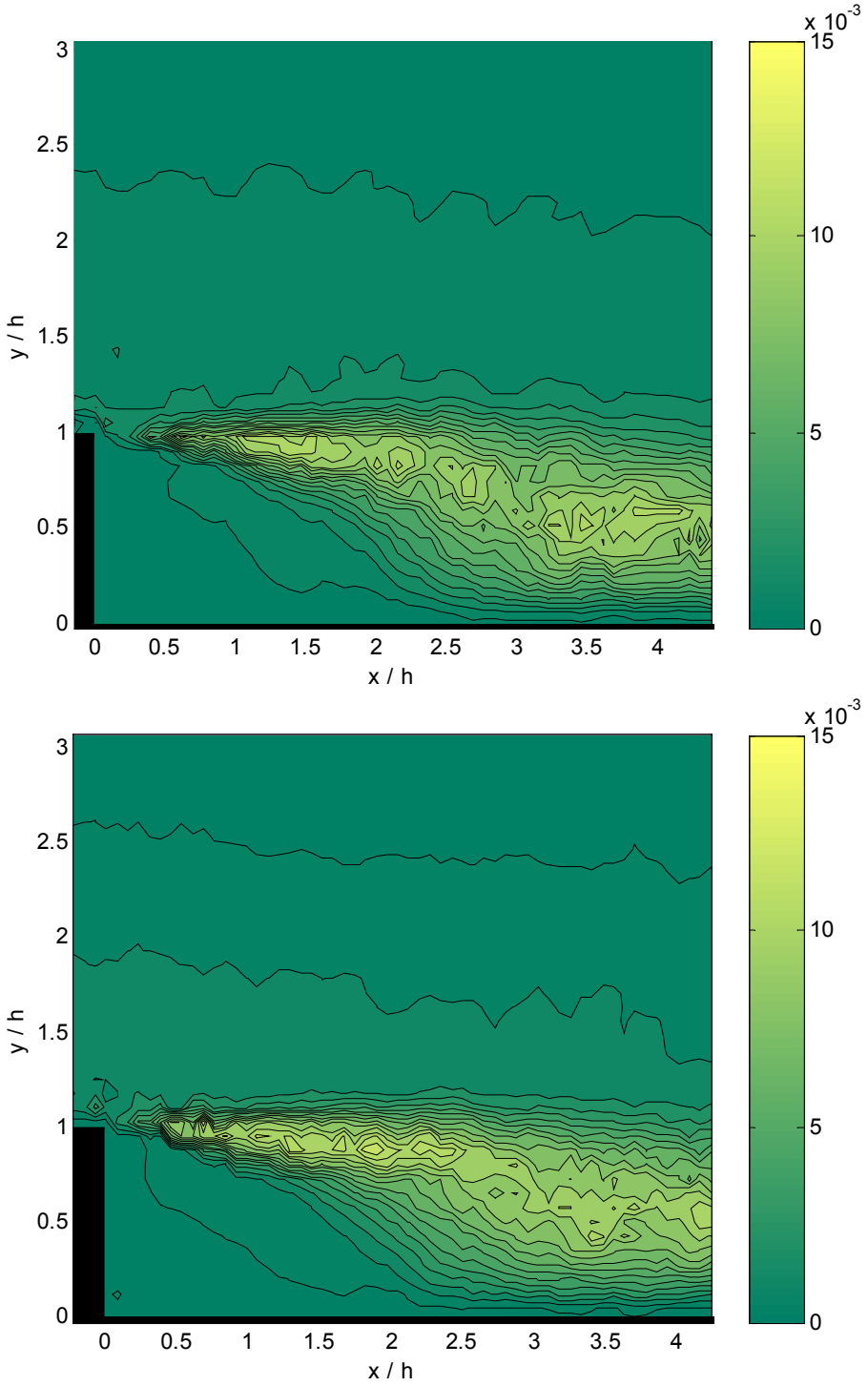

Figure 21. $-\overline{u'v'}/U_\infty^2$ **gray-scale contour maps for the 2D case $Re_h = 8081$, $W_s/U_\infty = 0$ (top) and the 3D case $Re_h = 8081$, $W_s/U_\infty = 0.48$ (bottom)**

The same trend can be seen when analyzing the gray-scale contour maps for the 2D and 3D cases at Re = 8081, which are displayed in Fig. 21. Notice that the magnitude of the Reynolds shear stress in the 3D case is slightly higher than the intensity of the $-\overline{u'v'}/U_\infty^2$ values in the 2D case. As previously mentioned, the reattachment distance in the 3D case is shorter than the reattachment distance for the 2D case. This suggests that a higher rate of momentum transport laterally in the 3D case is causing the shear layer to reattach at a shorter distance than the in the 2D case.

The individual $-\overline{u'v'}/U_\infty^2$ profiles in Fig. 22 for the same six different streamwise positions employed earlier to display u_{rms} and v_{rms} profiles provide a clearer support for the above observations. First looking at the 2D cases, the peak for the Re = 8081, 2D case near separation is almost double the magnitude of the peak for the Re = 32327, 2D case. This helps to support the idea that the shear layer, especially near separation, scales on u_τ and not U_∞ since the shear layer develops from the viscous stresses located in the near-wall region at separation. Throughout the shear layer, upstream of the reattachment as shown in the first four plots in Fig. 22, the lower Reynolds number 2D case has a larger Reynolds stress magnitude than the higher Re case. The gap between the two decreases, however, with increasing x/h distance. This again supports the conclusion of Morris and Foss[19] that a separating *turbulent* shear layer initially scales on the viscous stresses in the near-wall region at separation. Beyond reattachment, the two 2D case profiles collapse, which suggests that in this region $-\overline{u'v'}/U_\infty^2$ scales on U_∞. Comparing the individual profiles for the 2D and 3D cases at Re = 8081, near separation the peak in 3D case has a larger magnitude than the peak in 2D case. This indicates that there is a larger rate of lateral momentum transfer and in addition, the viscous stress in the near-wall region must also be greater in the 3D case than the 2D case. The gap between the two cases decreases with increasing distance from the step. In the x/h = 3.54 plot the two profiles collapse. From the observations made, it seems that the higher the $-\overline{u'v'}/U_\infty^2$ peak near separation, the shorter the reattachment distance due to more effective lateral momentum transfer near separation.

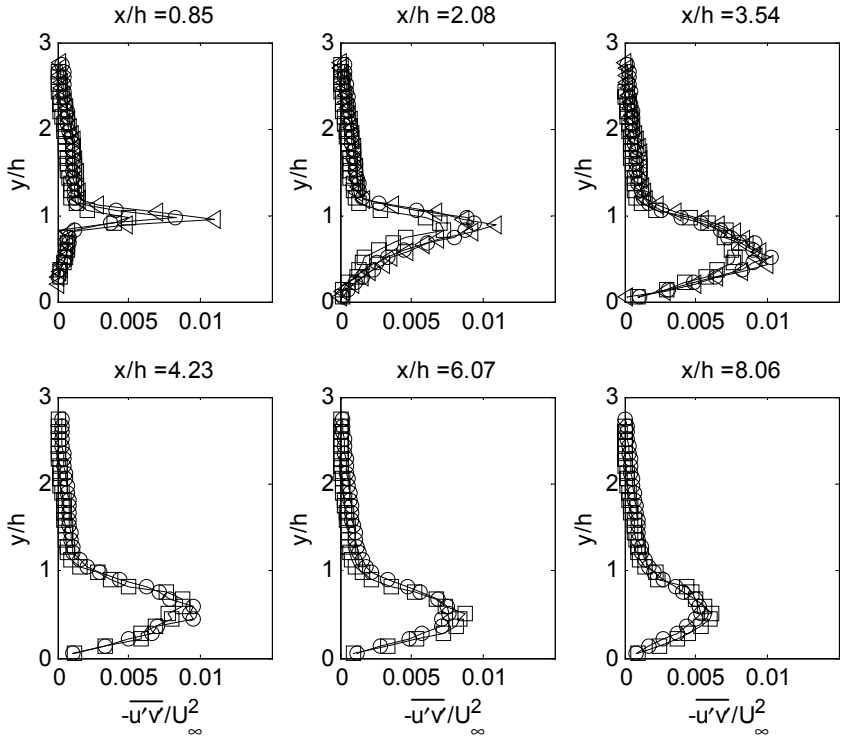

Figure 22. Reynolds shear stress profiles: (O)Re_h = 8081, W_s/U_∞ = 0.00, ( ) Re_h = 32327, W_s/U_∞ = 0.00, (◁) Re_h = 8081, W_s/U_∞ = 0.48

IV. Conclusion

An extensive planar PIV dataset of the flow field downstream of an axisymmetric backward-facing step was acquired for five different Reynolds numbers in the 2D separating boundary layer case. In addition, planar PIV data were acquired for two Reynolds numbers in the 3D separating boundary layer case; although only results for the Re_h = 8081 3D case were shown. Reynolds number effects have been investigated using a portion of the 2D data and a comparison between the 2D and 3D cases has been made.

An investigation into Reynolds number effects seen in the 2D data analysis was completed using mean and fluctuating velocity statistics. The mean velocity streamline plots and profiles of the shear layer and the recirculation zone above the wall revealed that both the reattachment length and the location of the secondary separation point are Reynolds number dependent. As Re_h increased, the reattachment distance grew while the secondary point moved closer to the step. The Reynolds number effect on the reattachment length was attributed to variation in the boundary layer momentum thickness as suggested earlier by Eaton and Johnston[2] and Adams and Johnston[8].

The streamwise and wall-normal turbulent rms velocity contour maps also indicated Reynolds number dependence near separation, where a peak in the turbulent intensity values was observed at x/h ~ 0.1 - 1. The existence of the peak may be explained by the findings of Morris and Foss[19], who suggested that the sub-shear layer region is dominated by viscous effects from the near-wall at separation. Nonetheless, this local maximum value near separation increased in magnitude with rising Reynolds number. A second peak was also identified in u_{rms} and v_{rms} contour maps. This peak was located slightly upstream of reattachment and increased slightly in magnitude with rising Re_h in u_{rms} maps and not in the v_{rms} maps. A noticeable characteristic change in the shape of the shear layer in the v_{rms} contour maps was observed at different Reynolds numbers. At lower Reynolds numbers such as Re = 8081, the shear layer was more spread out and the energy seemed to be diffusing out into the surrounding flow; whereas, at higher Reynolds numbers such as Re = 32327, the shear layer was more streamlined.

The effects of changing Reynolds number were also seen in the Reynolds stress contour maps. The magnitude of the Reynolds stress decreased with increasing Re_h, indicating that near separation $-\overline{u'v'}/U_\infty^2$ possibly scales on u_τ as suggested by Morris and Foss[19]. This observation, which requires further testing by directly measuring the wall-shear stress at separation, may provide an explanation for the increase seen in x_r for higher Re_h cases. At lower Reynolds numbers, the higher Reynolds stress values result in a higher rate of turbulent diffusion of momentum in the wall normal direction; whereas, at higher Reynolds number the momentum diffusion rate is lower as evidenced by the lower $-\overline{u'v'}/U_\infty^2$ values. This translates to a lower spread rate of the shear layer at higher Reynolds numbers, which leads to the longer reattachment length.

The comparison between the 2D and 3D cases showed some differences. The reattachment length was shorter in the 3D case than in the 2D case, which had a thicker boundary layer at separation than the 3D boundary layer. In addition, the local maximum peak seen in the turbulent intensity contour maps near separation increased in magnitude in the 3D case. This suggested that since the cross-flow was weak at separation, most of the three-dimensionality influence was limited to enhancing the turbulence activity in the initial development of the shear layer, but that the three-dimensionality effects died farther downstream; thus having no global influence on the separation bubble. Finally, the Reynolds stress values were greater in magnitude in the 3D case compared to the 2D case.

Acknowledgments

This work was sponsored by a grant through the National Science Foundation (Contract #CTS0116907), monitored by Dr. Mike Plesniak, with supplemental support from the Office of Naval Research, monitored by Dr. Ron Joslin. Any opinions, findings and conclusions or recommendations expressed in this material are those of the author(s) and do not necessarily reflect the views of the National Science Foundation and Office of Naval Research. The experiments were conducted under NASA Space Act Agreement (#SAA-1-562) on the Development and Application of Advanced Wall-Sensor-Arrays and Optical Diagnostics. In addition, L. M. Hudy was supported by funding through the NASA Harriett G. Jenkins Predoctoral Fellowship Program.

[1] Washburn, A. E., Gorton, S. A., and Anders, S. G., " Snapshot of Active Flow Control Research at NASA Langley," *1st AIAA Flow Control Conference*, AIAA 2002-3155, St. Louis, Missouri, June 24-26, 2002.

[2] Eaton, J. K. and Johnston, J.P., "A Review of Research on Subsonic Turbulent Flow Reattachment," *AIAA Journal*, Vol. 19, No. 9, 1981, pp. 1093-1099.

[3] Cherry, N. J., Hillier, R., Latour, M.E.M.P., "Unsteady Measurements in a Separated and Reattaching Flow," *Journal of Fluid Mechanics*, Vol. 144, 1984, pp. 13-46.
[4] Castro, I.P. and Haque, A., "The Structure of a Turbulent Shear Layer Bounding a Separation Region," *Journal of Fluid Mechanics*, Vol. 179, 1987, pp. 439-468.
[5] Hancock, P.E. and McCluskey, F. M., "Spanwise-Invariant Three-Dimensional Separated Flow," *Experimental Thermal and Fluid Science*, Vol. 14, 1997, pp. 25-34.
[6] Driver, D.M. and Hebbar, S.K. "Three-Dimensional Shear-Driven Boundary-Layer Flow with Streamwise Adverse Pressure Gradient," *AIAA Journal*, Vol. 27, No. 12, 1989, pp. 1689-1697.
[7] Li, Y. and Naguib, A.M., "A High-frequency Oscillating-hot-wire Sensor for Near-wall Diagnostics in Separated Flows," *42nd Aerospace Sciences Meeting & Exhibit*, AIAA 2004-1041, Reno, NV, January 5-8, 2004.
[8] Adams, E.W. and Johnston, J.P., "Effects of the separating shear layer on the reattachment flow structure, Part 2: Reattachment length and wall shear stress," *Experiments in Fluids*, Vol. 6, 1988, pp. 493-499.
[9] Spazzini, P.G., Iuso, G., Onorato, M., Zurlo, N., Di Cicca, G. M., "Unsteady behavior of back-facing step flow," *Experiments in Fluids*, Vol. 30, 2001, pp. 551-561.
[10] Kostas, J., Soria, J., and Chong, M.S., "Particle Image Velocimetry Measurements of a Backward-facing Step," *Experiments in Fluids*, Vol. 33, 2002, pp. 838-853.
[11] Scarano, F. and Riethmuller, M. L., "Iterative Multigrid Approach in PIV Image Processing with Discrete Window Offset," *Experiments in Fluids*, Vol. 26, 1999, pp. 513-523.
[12] Wernet, M.P., "Fuzzy logic enhanced digital PIV processing software", *18th International Congress on Instrumentation for Aerospace Simulation Facilities*, (ICIASF), Toulouse, France, June 1999.
[13] Meyers, J.F., "Doppler Global Velocimetry – The Next Generation?," *AIAA Paper 92-3897*, 1992.
[14] Wernet, M. P., *Particle Image Velocimetry Processing Manual PIVPROC*, NASA Glenn Research Center, Version 6.03, 2002.
[15] Dally, J. W., Riley, W. F., and McConnell, K. G., *Instrumentation for Engineering Measurements*, 2nd ed., John Wiley & Sons, Inc., New York, 1984, pp. 538.
[16] Eaton, J. K., "Turbulent flow reattachment: an experimental study of the flow and structure behind a backward-facing step," Ph.D. Dissertation, Stanford University, 1980.
[17] Westphal, R.V. and Johnston, J.P., "Effect of initial conditions on turbulent reattament downstream of a backward-facing step," *AIAA Journal*, Vol. 22, 1984, pp. 1727-1732.
[18] Tihon, J., Legrand, J., and Legentilhomme, P., "Near-wall investigation of backward-facing step flows," *Experiments in Fluids*, Vol. 31, 2001, pp. 484-493.
[19] Morris S. C., and Foss, J. F., "Turbulent boundary layer to single-stream shear layer: the transition region," *Journal of Fluid Mechanics*, Vol. 494, 2003, pp. 187-221.
[20] Ruderich, R. and Fernholz, H. H., "An Experimental Investigation of a Turbulent Shear Flow with Separation, Reverse Flow, and Reattachment," *Journal of Fluid Mechanics*, Vol. 163, 1986, pp. 283-322.
[21] Huang, H.T. and Fiedler, H. E., "A DPIV Study of a Starting Flow Downstream of a Backward-facing Step," *Experiments in Fluids*, Vol. 23, 1997, pp. 395-404.
[22] Heenan, A.F. and Morrison, J. F., "Passive Control of Pressure Fluctuations Generated by Separated Flow," *AIAA Journal*, Vol. 36, 1998, pp. 1014-1022.